Structure of the FeBTC Metal-Organic Framework: a Model Based on the Local Environment Study.

Luisa Sciortino, Antonino Alessi, Fabrizio Messina, Gianpiero Buscarino, Franco Mario Gelardi.*

Dipartimento di Fisica e Chimica, Università degli Studi di Palermo, Via Archirafi 36, 90123 PA, Italy

AUTHOR INFORMATION

Corresponding Author

* Gianpiero Buscarino gianpiero.buscarino@unipa.it

ABSTRACT The local environment of iron in FeBTC, a metal organic framework commercially known as Basolite F300, is investigated combining XANES and EXAFS studies of the iron K-edge. The building block of the FeBTC can be described as an iron acetate moiety. Dehydration induces a change in the coordination of the first shell while preserving the network. We propose that the local structure around Fe atoms does not undergo a rearrangement, thus leading to the formation of an open site. The analysis conveys that the FeBTC is a disordered network of locally ordered blocks.

KEYWORDS MOF, Iron based MOF, XAFS, Fe K-edge, Fe K-pre edge.

INTRODUCTION

Metal-Organic Frameworks (MOF) are a class of materials consisting of metal building units coordinated by organic moieties to form an extended regular one, two, or three dimensional structure. [1] Their extraordinary porosity and their chemically tunable structures make them, to date, the most promising materials for several applications such as gas storage [2,3] and separation, [4] drug delivery [5] and sensors. [6,7] Nowadays, one of their main utilities remains undoubtedly catalysis [8,9] mainly occurring at active sites, formed when the MOF is dehydrated by what is commonly named an activation process.

Due to the low toxicity and the high biocompatibility of iron, an increase in the use of iron-based MOFs is widely regarded as a highly desirable target. [10] A required step to accomplish this goal is to significantly improve our current understanding of their properties, hence the ability to control them. FeBTC, also known as Basolite F300, is nominally constituted by iron building units connecting 1,3,5 BenzeneTriCarboxylic acid (BTC also called trimesic acid) linkers. FeBTC (empirical formula $C_9H_3FeO_6$) is widely available, features a pore dimension of 22 Å and a BET surface of 1500 m^2/g, [11] and exhibits high catalytic activity for a large variety of organic transformations. [12] The oxidation state of iron atoms is found to be +3 [13,14] but the local environment around iron is still unsettled. Indeed, in contrast to other well-known commercial MOFs as HKUST-1 [15] (Copper 1,3,5 benzenetricarboxylate) the structure of FeBTC remains largely unknown, mainly because of its poor cristallinity: in this regards FeBTC has been described in literature as being neither crystalline nor amorphous but, rather, disordered. [13] Such description does not get over the structural problem and, rather, the issue remains unresolved. In sharp contrast with FeBTC, the structure of the MIL-100(Fe), which is considered the equivalent crystalline iron trimesate, is well defined and has been characterized by synchrotron X-ray

powder diffraction, indicating a zeolitic structure built up by trimers of iron octahedra sharing a common vertex (μ_3-O) and linked by 1,3,5 benzenetricarboxylic moieties. [16,17] Recently, it was demonstrated that commercial FeBTC is suitable as heterogeneous catalyst when a strong Lewis acid site is required. [13] Although FeBTC and MIL-100(Fe) show comparable concentrations of Lewis acid sites, the catalytic activity of FeBTC is surprisingly higher and does not appear to correlate with the density and strength of Lewis acid sites, that are associated with coordination positions of iron ions. In aerobic oxidation reaction FeBTC is found to be very selective with respect to other commercial MOFs as HKUST-1. [18] In this respect, resolving the structure of FeBTC and elucidating the local environment of Fe atoms in the hydrated and activated state is a vital prerequisite to understand the catalytic cycles.

Here we studied the exposed to air and activated FeBTC by X-ray absorption (XAS) in the iron K-edge region. The oxidation state and the local geometry are revealed by the X-ray Absorption Near Edge Structure (XANES) data and the distances and coordination numbers are modeled analyzing the Extended X-ray Absorption Fine Structure (EXAFS) region. From the analysis of XAS data we find that the FeBTC structure is constituted by iron acetate motif where all metallic atoms are linked to 1,3,5 benzenetricarboxylic acid.

RESULTS AND DISCUSSION

We report in figure 1 the X-ray absorption spectra of FeBTC in the XANES region. Comparing the position E_0, the absorption edge energy, of the activated FeBTC with that observed in reference materials with different Fe oxidation states readily suggests that iron atoms in FeBTC are essentially in the +3 oxidation state. Besides, the XANES signal of exposed to air FeBTC and activated FeBTC are compared in fig.1 as well and appear indeed very similar in

regard of the position of the E_0 and of the shape of the absorption spectrum near the edge. Finally, here and after, no changes are observed between a sample exposed for 24 hours to air (data shown in figure 1) and a sample measured as-received (data are reported in the Supporting information fig.S1-S3). Overall, at this level of analysis, one can exclude that the exposure to air or the activation induces strong changes of either the local environment or the oxidation state of iron. In other words FeBTC is rather stable and it is not susceptible to dramatic changes when the atmosphere is modified from air to vacuum or when adsorbed water molecules are removed by activation.

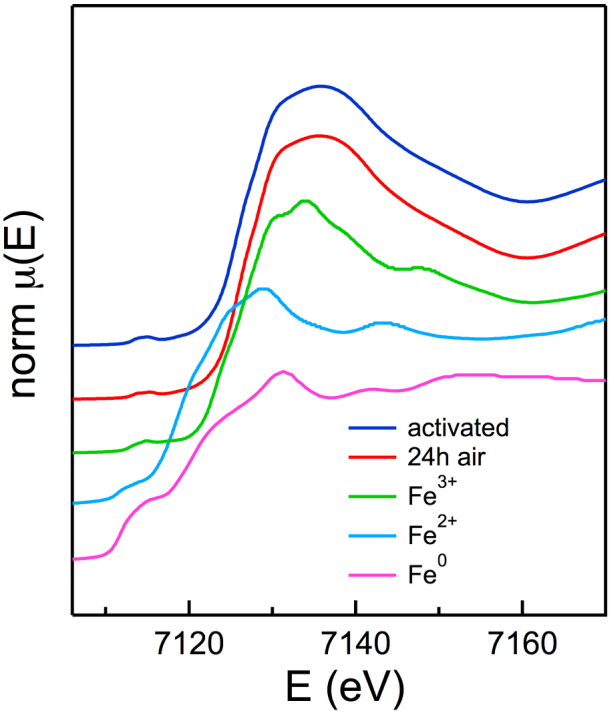

Figure 1. XANES spectra of 24h air (red) and activated (blue). FeBTC samples are compared with references containing iron in +3 state (Fe_2O_3 green), in +2 state (FeO light blue) and in the 0 oxidation state (metallic iron, magenta). Signals are shifted along the y-axis for clarity.

In figure 2 we show a zoom of the XANES spectra of FeBTC in the pre-edge spectral region, and compare these data to those obtained in Fe(II) and the Fe(III) reference compounds. The well-defined absorption feature clearly visible in all spectra is characteristic of the Fe K-edge and is known to arise from the 1s -> 3d transition. [19] The superimposition of the pre-edge of the sample and reference signals bring to an analogous result coming from the comparison between the edge positions (fig.1). Noticeably, both the shape and the position of the pre-edge of the experimental data are in agreement to the signal of Fe^{3+} and don't fit the Fe^{2+} signal.

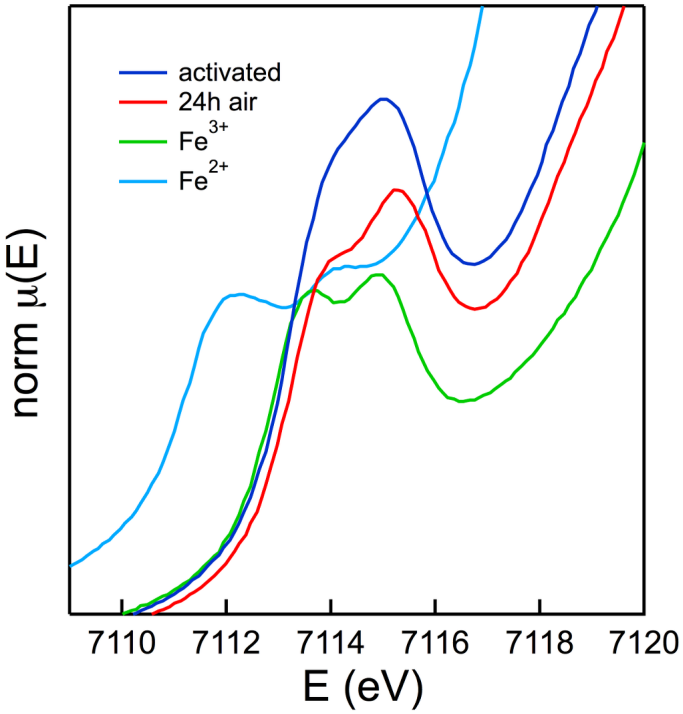

Figure 2. XANES Pre-edge of samples and references. Spectra of 24h air (red), and activated (blue) are compared with references containing iron in +3 state ($Fe_2(SO_4)_3$ green), and in +2 state ($FeSO_4$ light blue).

In Figure 3, the normalized (as described in the experimental section to directly compare the areas) pre-edge absorptions of the two FeBTC samples are reported. As explained hereafter,

analysis of these pre-edge data not only reinforces our above assignment of the oxidation state of iron, but it also reveals fine details on the effect of activation, and provides precise information on the local symmetry around iron.

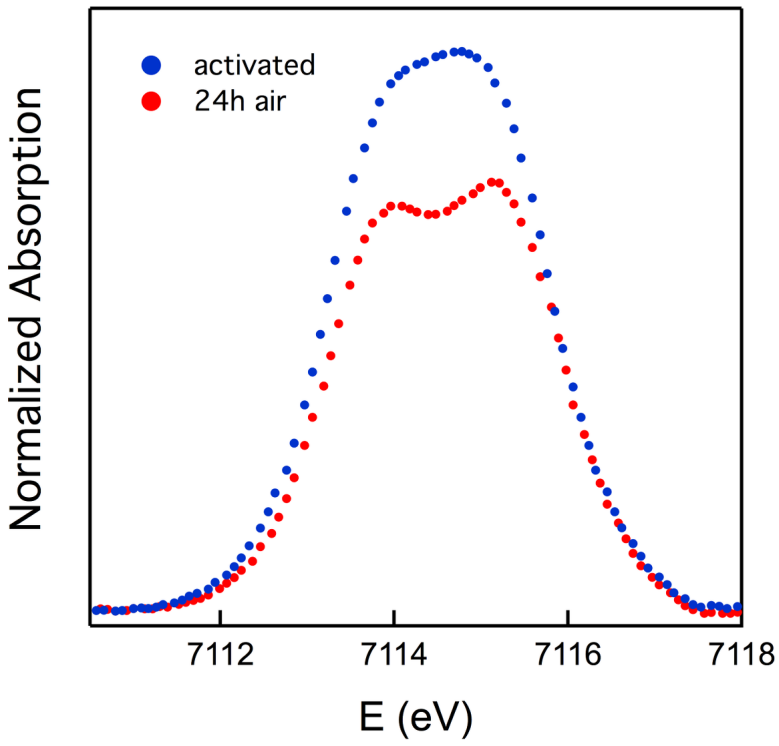

Figure 3. XANES Normalized pre-edge of 24h air (red dots) and activated (blue dots) FeBTC, the normalization is carried out using the procedure described in the experimental section.

Indeed, the centroid position of the pre-edge 1s->3d absorption is sensitive to the oxidation state, being splitted by 2 eV for the Fe^{2+} and Fe^{3+} state, [20] being the Fe^{2+} at lower energy. These two characteristic positions fairly agree with our data on the two reference materials. Notably, the 1s->3d transition is dipole-forbidden in a rigorously centrosymmetric environment, but becomes partially allowed when a lowering of the symmetry induces a mixing of 3d and 4p orbitals (because the transition 1s->4p is dipole-allowed). Thus, pre-edge absorption is stronger

in a tetrahedral geometry, lacking a center of inversion, than for an octahedral site endowed with higher symmetry. [21] More generally, the area of the pre-edge peak normally increases when the occupancy of d-orbital decreases and when the degree of symmetry decreases. [22] Notably, the relationship between geometry and pre-edge absorption shape was extensively analyzed in studies on volcanic glasses, with the following results: for Fe(III) in an octahedral site, two different electronic transitions are foreseen to stem from the 1s core orbital with an expected energy separation of about 1.5 eV (Δo) due to the octahedral crystal field. [20] On the contrary, the energy separation due to tetrahedral crystal field (Δt) is sensibly smaller, and predicted to be $4/9\Delta o$ corresponding to about 0.67 eV. On these grounds, comparing (Fig. 2) the pre-edge of FeBTC samples with Fe(II) and Fe(III) reference samples highlights that the centroid position of the pre-edge feature of FeBTC is unarguably ascribable to Fe^{3+} iron. This confirms that Fe atoms in FeBTC are in the higher +3 oxidation state, as already suggested above based on the edge position (Fig. 1) and from literature. [13] Furthermore, the pre-edge absorption measured in 24h air FeBTC shows two peaks with an energy separation equal to 1.2 eV. The presence of two recognizable peaks suggests that the local symmetry experienced by iron atoms in FeBTC is very close to octahedral, although the reported value for slightly distorted octahedra is 1.5 eV [20] which can be due to different extents of distortion. Finally, data in Fig. 3 show that the pre-edge area for the activated sample is 1.2 times larger than the 24h air sample, while after the activation process the spectral positions of the two observable peaks are so closer, that are not resolved. The signal appears as only one peak as foreseen for a low symmetry environment. [20]

Both these effects can be ascribed to the dehydration; in fact the removal of the water molecules, naturally contained in air, around the iron sites causes a reduction in d- orbital

occupancy and a lowering of the symmetry degree that gives rise to decreased separation of the pre-edge peaks.

Overall, XANES spectra point out the prevalence of Fe(III) both in samples stored in air and in the activated sample. The ligands around iron are arranged in octahedral geometry, with a reduction of the d-orbital occupancy after the activation.

To resolve the local structure around Fe in FeBTC the EXAFS signal of the 24h air, and the activated samples are investigated. An equivalent study for the as received sample is reported in Supporting Information file. The EXAFS spectra of all samples can be directly compared (fig.S4) showing that the activated and the 24h air FeBTC are similar in terms of oscillation positions but differ for oscillation amplitudes, that are strictly correlated to coordination numbers. [23] Due to the nature of the ligands and of the metal we propose that the building block of FeBTC closely resembles the iron(III) acetate. Then basing on the identified lattice structure of MIL-100(Fe), [16] of the proposed local structure for other iron-based MOFs, [24] both underpinned on iron acetate, and on our findings from XANES analysis, a simple model for the EXAFS analysis is built up. The structure we propose, hereafter named Acetate-Model, can be depicted as $Fe_3(\mu_3\text{-}O)(\mu\text{-}OAc)_6(H_2O)_3$ moiety, where Ac is the CH_3CO group (fig.4 left panel).

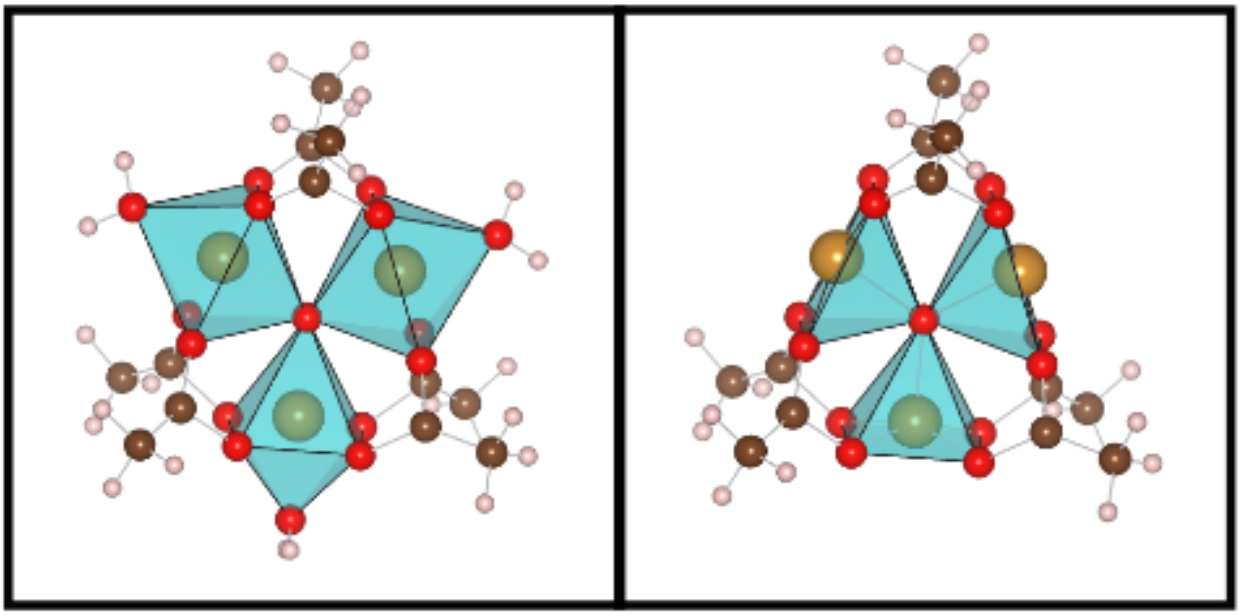

Figure 4. Acetate-Model picture where iron atoms are inside the polyhedra, oxygen atoms are red, carbon atoms are brown, and hydrogen atoms are white. Left panel: the Acetate-Model built up to fit the EXAFS. Right panel: the dehydrated Acetate-Model.

The model contains three equivalent iron atoms each bound to six oxygen ligands in octahedral geometry. A trimer of iron octahedra shares a common vertex μ_3-O, while the four ligands, that are located at the equatorial plane, are bidentate acetate bridging two iron atoms, and the last one is the oxygen of the water molecule.

The iron atom subjected to photoelectron phenomena is labeled as Fe^{abs}. The scattering atoms are (i) the six oxygen atoms (O^1) directly bonded to Fe^{abs}, one belonging to the water molecule, the four nearest carboxyl groups, and the shared oxygen between the three octahedra. Other scatterers are (ii) the four carbon atoms marked (C^1) of the nearest carboxyl groups, the (iii) two iron (Fe^1), of the nearest octahedra, (iv) the other four oxygen atoms, O^2, of the carboxyl groups, and (v) the carbon and oxygen atoms, C/O^m, of the carboxyl groups in front to the absorber.

After a rigorous analysis of the scattering paths that are generated for the $Fe_3(\mu_3\text{-}O)(\mu\text{-}OAc)_6(H_2O)_3$ structure, only five single paths give an essential contribution to well-describe the local environment of the iron. The graphical description of the chosen paths is reported in fig.5 and the fitting procedure in the supporting information file.

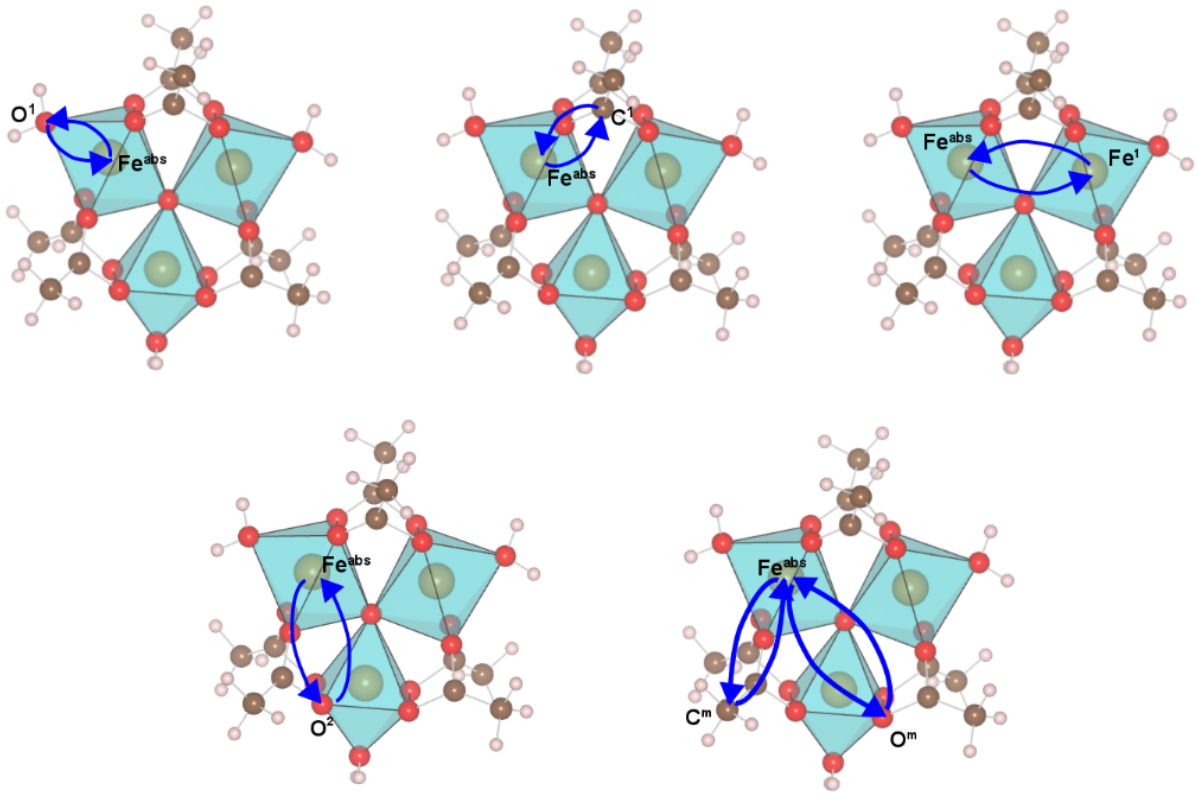

Figure 5. Scattering paths of the photoelectron for the EXAFS analysis.

First, the coordination numbers for all paths were fixed to the ideal values, then the fitting parameters were refined to obtain the best fits. The numerical results from the best fits are summarized in table 1.

Table 1. Quantitative Results of the EXAFS Data Analysis of FeBTC measured after 24 hours of exposure to air (Top), and after the activation (Bottom).[a]

Scattering path	N_{Coor}	R(Å)	$\sigma^2(Å^2)$
24h air sample			
Fe^{abs}-O^1	5.2	2.00	0.006
Fe^{abs}-C^1	3.5	2.99	0.004
Fe^{abs}-Fe^1	2.2	3.06	0.026
Fe^{abs}-O^2	4.3	3.33	0.004
Fe^{abs}-C/O^m	7.9	3.99	0.025
activated sample			
Fe^{abs}-O^1	4.7	1.99	0.007
Fe^{abs}-C^1	3.5	2.99	0.006
Fe^{abs}-Fe^1	2.2	3.07	0.029
Fe^{abs}-O^2	4.3	3.33	0.007
Fe^{abs}-C/O^m	7.2	4.00	0.027

[a]For the five scattering paths used to simulate the experimental curve, the table reports the optimized parameters: (i) the coordination number (NCoor); (ii) the absorber to scatterer distance (R); and (iii) the Debye-Waller factor (σ2). Uncertainty is 10% for NCoor, 0.02 Å for R, and on the last digit for σ2.

The goodness of the fit is appreciable in figure 6 for the 24h air sample and in figures S5-S10 (see Supporting information file). By inspection of Table 1, the interatomic distances between absorber and scatterers before and after the dehydration are mostly unchanged. Regarding the coordination numbers the alteration of the Fe^{abs}-O^1 path is detectable: the number of oxygen ligands decreases when the sample is activated although other parameters remain unchanged. For these reasons a modification of the Acetate-Model (fig.4 right panel) is taken into account for the activated sample. A fraction of the water ligands are eliminated forasmuch as the water molecules are removed through the activation process. The findings, that the distances and the coordination numbers are comparable in presence or not of water, support the hypothesis of a

rigid structure around iron. After the activation the structure slightly relaxes keeping intact the building block of acetate-model.

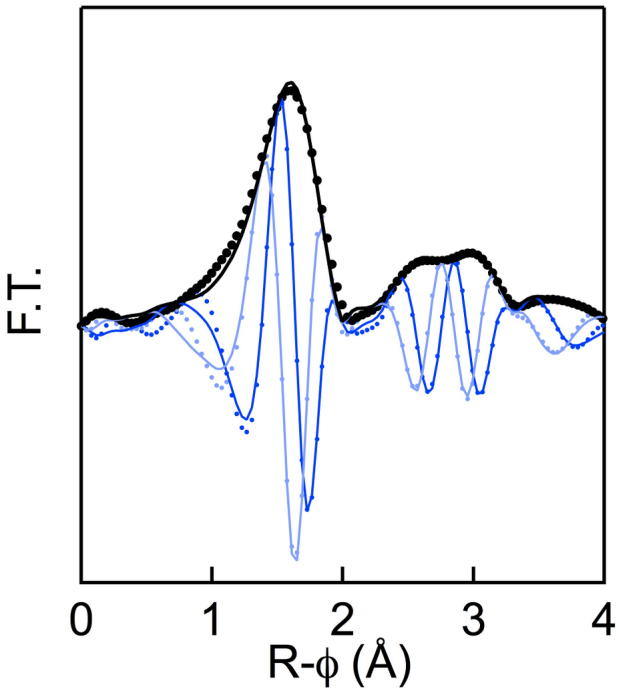

Figure 6. Fourier transform of EXAFS data collected on the 24h air sample. The refinement is carried out including all N_{Coor}. Points are the experimental data and the lines are the best fit curves. The different colors correspond to the module (black), the real component (dark blue), and the imaginary component (light blue), respectively.

The structure does not rearrange generating an open metal site that explains the Lewis acidity. Nevertheless, the high catalytic activity of the FeBTC was justified by the presence of additional Brönsted acid sites [13] that are likely placed at a significant distance from iron atoms, or otherwise the local environment of iron would be affected. Indeed, we propose that the Brönsted acid sites are constituted of terminal carboxyl groups whose presence interrupts the order of the network giving rise to a MOF with low cristallinity, clearly testified by the X-ray Diffraction pattern

reported in fig.S11. Overall, the XAFS analysis allows describing the FeBTC as a disordered network of locally ordered units composed by acetate-model moieties with Fe^{3+} irons.

EXPERIMENTAL SECTION

All materials were purchased from Sigma Aldrich and used without purification. The XAFS spectra of the following standards, used for reference purposes, were collected at liquid nitrogen (LN) temperature: Fe foil (thickness 4 μm), FeO, Fe_2O_3, $FeSO_4$, and $Fe_2(SO_4)_3$. The samples were measured using the same experimental parameters for the reference spectra. FeBTC was studied in three different conditions: (i) the FeBTC as purchased from the Sigma Aldrich called "as received", (ii) the FeBTC after 24 hours of exposure of the as received to air called "24h air", and (iii) the activated FeBTC named "activated". The process of activation, carried out in a laboratory at ELETTRA synchrotron, consisted of a thermal treatment in oven kept at 393 K in vacuum for several hours (at least 3 hours) thereby the water molecules are desorbed and the structure is still preserved. These conditions were chosen basing on previously published TGA (ThermoGravimetic Analysis). [13] The activated sample was measured right afterwards the thermal treatment to avoid the rehydration of FeBTC. Samples and references, except for the foil, were mixed with Boron nitride and pressed at 3 tons. All specimens were placed in a sample holder with kapton windows.

The X-ray absorption measurements were recorded at the XAFS beamline of the Elettra synchrotron radiation facility, Trieste, where the synchrotron radiation emitted by a bending magnet source was monochromatized using a double crystal Si(111) (with energy resolution $\approx 2*10^{-4}$). We have performed the XANES and the EXAFS measurements in transmission geometry on the K-edge of the iron (7112 eV) using two ionization chambers filled with a N2/Ar

mixture at different composition for the incident I_0 and transmitted I_1 beam, respectively. The measurements were recorded with an integration time of 2 s in the 6812-8635 eV range using a pre-edge step of 5 eV, a step 0.10 eV for the acquisition of the edge, and a k constant step of 0.03 $Å^{-1}$ for the EXAFS region. XANES spectra were also acquired for Fe foil as an internal standard reference for energy calibration. All shown data are an average of three different measures. The absorption spectra were collected in vacuum atmosphere ($p=6.6*10^{-4}$ bar) at LN temperature to limit the thermal disorder effects, which damp the EXAFS oscillations, thus allowing the collection of high quality data in a wide range of k.

XANES spectra were normalized by subtracting an *arctangent* function from the data and normalizing with respect to the edge jump height.[25] The EXAFS spectra were analyzed with Feff [26] and Viper [27] fitting both real and imaginary components of the data in R-space (1.3-3.8 Å) in single scattering approximation.

ASSOCIATED CONTENT

Further details about experimental spectra, fitting procedure, and XRD (X-Ray Diffraction) pattern are available in Supporting Information file. This material is available free of charge via the Internet at http://pubs.acs.org.

AUTHOR INFORMATION

Corresponding author

*gianpiero.buscarino@unipa.it

NOTES

The Authors declare no competing financial interest

ACKNOWLEDGEMENT

We acknowledge the Elettra Sincrotrone Trieste (proposal 20130414) for provision of synchrotron facilities and we thank Luca Olivi of the Staff of the XAFS beamline of Elettra for assistance. Furthermore, we acknowledge the LAMP group (www.unipa.it/lamp) for stimulating discussion and useful advices.

REFERENCES

(1) Rowsell J.L.C. and Yaghi O.M. Metal–Organic Frameworks: a New Class of Porous Materials. *Micropor. Mesopor. Mat.* **2004**, *73*, 3–14.

(2) Latroche, M.; Surblé, S.; Serre, C.; Mellot-Draznieks, C.; Llewellyn, P.L.; Lee, J.; Chang, J.; Jhung, S.H.; Férey, G. Hydrogen Storage in the Giant-Pore Metal–Organic Frameworks MIL-100 and MIL-101. *Angew. Chem. Int. Edit.* **2006**, *45*, 8227–8231.

(3) Tranchemontangne, D.J.; Sung Park, K.; Furukawa, H.; Eckert, J.; Knobler, C.B.; Yaghi O.M.; J. Hydrogen Storage in New Metal–Organic Frameworks. *Phys. Chem. C* **2012**, *116*, 13143–13151.

(4) Li, J.R.; Sculley, J.; and Zhou, H.C. Metal–Organic Frameworks for Separations. *Chem. Rev.* **2012**, *112*, 869–932.

(5) McKinlay, A.C.; Morris, R.E.; Horcajada, P.; Férey, G.; Gref, R.; Couvreur, P.; Serre, C. BioMOFs: Metal–Organic Frameworks for Biological and Medical Applications. *Angew. Chem. Int. Edit.* **2010**, *49*, 6260–6266.

(6) Takashima, Y.; Martínez Martínez, V.; Furukawa, S.; Kondo, M.; Shimomura, S.; Uehara, H.; Nakahama, M.; Sugimoto, K.; Kitagawa, S. Molecular Decoding Using Luminescence From an Entangled Porous Framework. *Nat. Commun.* **2011**, *2*:168.

(7) Kreno, L.E.; Leong, K.; Farha, O.K.; Allendorf, M.; Van Duyne, R.P.; Hupp, J.T. Metal–Organic Framework Materials as Chemical Sensors. *Chem. Rev.* **2012,** *112*, 1105–1125.

(8) Lee, J.; Farha, O.K.; Roberts, J.; Scheidt, K.A.; Nguyen S.T.; Hupp, J.T. Metal–Organic Framework Materials as Catalysts. *Chem. Soc. Rev.* **2009**, *38*, 1450-1459.

(9) Laurier, K.G.M.; Vermoortele, F.; Ameloot, R.; De Vos, D.E.; Hofkens, J.; Roeffaers M.B.J. Iron (III)-Based Metal–Organic Frameworks as Visible Light Photocatalysts. *J. Am. Chem. Soc.* **2013**, *135*, 14488–14.

(10) Horcajada, P.; Chalati, T.; C Serre, C.; Gillet, B.; Sebrie, C.; Baati, T.; Eubank, J.F.; Heurtaux, D.; Clayette, P.; Kreuz, C.; et al. R. Porous Metal–Organic-Framework Nanoscale Carriers as a Potential Platform for Drug Delivery and Imaging. *Nat. Mater.* **2010**, *9*, 172–178.

(11) Babu, F.K.; Kulandainathan, M.A.; Katsounaros, I.; Rassaei, L.; Burrows, A.D.; Raithby, P.R.; Marken, F. Electrocatalytic Activity of Basolite TM F300 Metal-Organic-Framework Structures. *Electrochem. Commun.* **2010**, *12*, 632–635.

(12) Dhakshinamoorthy, A.; Alvaro, M.; Chevreau, H.; Horcajada, P.; Devic, T.; Serre, C.; Garcia, H. Iron(III) Metal–Organic Frameworks as Solid Lewis Acids for the Isomerization of α-Pinene Oxide. *Catal. Sci. Technol.* **2012**, *2*, 324–330.

(13) Dhakshinamoorthy A.; Alvaro, M.; Horcajada, P.; Gibson, E.; Vishnuvarthan, M.; Vimont, A.; Grenèche, J.M.; Derre C.; Daturi, M.; Garcia H. Comparison of Porous Iron Trimesates Basolite F300 and MIL-100(Fe) As Heterogeneous Catalysts for Lewis Acid and Oxidation Reactions: Roles of Structural Defects and Stability. *ACS Catal.* **2012**, *2*, 2060–2065.

(14) Dhakshinamoorthy, A.; Alvaro, M.; Garcia, H. Atmospheric-Pressure, Liquid-Phase, Selective Aerobic Oxidation of Alkanes Catalysed by Metal–Organic Frameworks. *Chem. Eur. J.* **2011**, *17*, 6256–6262.

(15) Prestipino C.; Regli, L.; Vitillo, J,G.; Bonino, F.; Damin, A.; Lamberti, C.; Zecchina, A.; Solari, P.L.; Kongshaug, K.O.; Bordiga, S. Local Structure of Framework Cu(II) in HKUST-1 Metallorganic Framework: Spectroscopic Characterization upon Activation and Interaction with Adsorbates. *Chem. Mater.* **2006**, *18*, 1337-1346.

(16) Horcajada, P.; Surblé, S.; Serre, C.; Hong, D.Y.; Seo, Y.K.; Chang, J.S.; Grenèche, J.M.; Margiolaki, I.; Férey, G. Synthesis and Catalytic Properties of MIL-100 (Fe), an Iron (III) Carboxylate with Large Pores. *Chem. Commun.* **2007**, 2820-2822.

(17) Birsa Čelič, T.; Rangus, M., Lázár; K., Kaučič; V., Zabukovec Logar, N. Spectroscopic Evidence for the Structure Directing Role of the Solvent in the Synthesis of Two Iron Carboxylates. *Angew. Chem. Ed. Int.* **2012**, *51*, 12490-12494.

(18) Dhakshinamoorthy, A.; Alvaro, M.; Garcia, H. Metal Organic Frameworks as Efficient Heterogeneous Catalysts for the Oxidation of Benzylic Compounds with t-Butylhydroperoxide. *J. Catal.* **2009**, *267*, 1–4.

(19) DeBeer George, S.; Petrenko, T.; Neese, F. Prediction of Iron K-Edge Absorption Spectra Using Time-Dependent Density Functional Theory. *J. Phys. Chem. A* **2008**, *112*, 12936–12943.

(20) Galoisy, L.; Calas, G.; Arrio. M.A. High-resolution XANES Spectra of Iron in Minerals and Glasses: Structural Information from the Pre-edge Region. *Chem. Geol.* **2001**, *174*, 307–319.

(21) Westre, T.E.; Kennepohl, P.; DeWitt, J.G.; Hedman, B.; Hodgson, K.O.; Solomon, E.I. A Multiplet Analysis of Fe K-edge 1s→ 3d Pre-edge Features of Iron Complexes. *J. Am. Chem. Soc.* **1997**, *119*, 6297-6314.

(22) Jackson, W.E.; Farges, F.; Yeager, M.; Mabrouk, P.A.; Rossano, S.; Waychunas, G.A.; Solomon, E.I.; Brown Jr. G.E. Multi-Spectroscopic Study of Fe (II) in Silicate Glasses: Implications for the Coordination Environment of Fe (II) in Silicate Melts. *Geochim. Cosmochim. Ac.* **2005**, *69*, 4315–4332.

(23) Lengeler, B.; Eisenberger, P. Extended X-ray Absorption Fine Structure Analysis of Interatomic Distances, Coordination Numbers, and Mean Relative Displacements in Disordered Alloys. *Phys. Rev. B* **1980**, *21*, 4507-4520.

(24) Surblé S.; Millange F.; Serre C.; Férey G.; Walton I. An EXAFS Study of the Formation of a Nanoporous Metal–Organic Framework: Evidence for the Retention of Secondary Building Units During Synthesis. *Chem. Commun.* **2006**, 1518-1520.

(25) Randall C.R.; Shu L.; Chiou Y.; Hagen K.S.; Ito M.; Kitajima N.; Lachicotte, R.J.; Zang Y.; Que L. Jr. X-ray Absorption Pre-Edge Studies of High-spin Iron (II) Complexes. *Inorg. Chem.* **1995**, *34*, 1036-1039.

(26) Ankudinov, A. L.; Ravel, B.; Rehr, J.J.; Conradson, S.D. Real-Space Multiple-Scattering Calculation and Interpretation of X-ray Absorption Near-Edge structure. *Phys. Rev. B*, **1998**, *58*, 7565-7576.

(27) Klementev, K.D. Viper:Freeware. *J. Phys. D: Appl. Phys.* **2001**, *34*, 209.

TOC GRAPHICS